American Mineralogist, Volume 105, pages 1769–1777, 2020

Phase transitions in ε-FeOOH at high pressure and ambient temperature

Elizabeth C. Thompson[1,*,†], Anne H. Davis[2], Nigel M. Brauser[2], Zhenxian Liu[3], Vitali B. Prakapenka[4], and Andrew J. Campbell[2]

[1]Department of Earth and Environmental Systems, The University of the South, Sewanee, Tennessee 37383, U.S.A.
[2]Department of the Geophysical Sciences, University of Chicago, Chicago, Illinois 60637, U.S.A.
[3]Department of Physics, University of Illinois, Chicago, Illinois 60607, U.S.A.
[4]Center for Advanced Radiation Sources, University of Chicago, Chicago, Illinois 60637, U.S.A.

Abstract

Constraining the accommodation, distribution, and circulation of hydrogen in the Earth's interior is vital to our broader understanding of the deep Earth due to the significant influence of hydrogen on the material and rheological properties of minerals. Recently, a great deal of attention has been paid to the high-pressure polymorphs of FeOOH (space groups $P2_1nm$ and $Pnnm$). These structures potentially form a hydrogen-bearing solid solution with AlOOH and phase H ($MgSiO_4H_2$) that may transport water (OH^-) deep into the Earth's lower mantle. Additionally, the pyrite-type polymorph (space group $Pa\bar{3}$ of FeOOH), and its potential dehydration have been linked to phenomena as diverse as the introduction of hydrogen into the outer core (Nishi et al. 2017), the formation of ultralow-velocity zones (ULVZs) (Liu et al. 2017), and the Great Oxidation Event (Hu et al. 2016). In this study, the high-pressure evolution of FeOOH was re-evaluated up to ~75 GPa using a combination of synchrotron-based X-ray diffraction (XRD), Fourier transform infrared spectroscopy (FTIR), and optical absorption spectroscopy. Based on these measurements, we report three principal findings: (1) pressure-induced changes in hydrogen bonding (proton disordering or hydrogen bond symmetrization) occur at substantially lower pressures in ε-FeOOH than previously reported and are unlikely to be linked to the high-spin to low-spin transition; (2) ε-FeOOH undergoes a 10% volume collapse coincident with an isostructural $Pnnm \rightarrow Pnnm$ transition at approximately 45 GPa; and (3) a pressure-induced band gap reduction is observed in FeOOH at pressures consistent with the previously reported spin transition (40 to 50 GPa).

Keywords: Phase transitions, infrared-spectroscopy, optical absorption spectroscopy, X-ray diffraction, spin transition; Volatile Elements in Differentiated Planetary Interiors

Introduction

The accommodation, distribution, and circulation of hydrogen in the deep Earth is key to understanding the evolution of Earth's interior due to the significant influence of hydrogen on the material and rheological properties of high-pressure phases (e.g., Sarafian et al. 2017; Karato 2010). Geophysical observations indicate that the Earth's upper mantle and transition zone, at least locally, host significant quantities of hydrogen (van der Meijde et al. 2003; Dixon et al. 2004; Pearson et al. 2014; Palot et al. 2016; Tschauner et al. 2018). Additionally, tomographic evidence supports the idea that subducting lithospheric plates pierce the transition zone, potentially ushering water into the Earth's lower mantle (van der Hilst et al. 1997). Yet while hydrogen in the upper mantle and transition zone is hosted primarily in nominally anhydrous phases, these phases are not stable at the high pressure and temperature conditions of the lower mantle (Hirschmann 2006). If hydrogen introduced into the lower mantle remains in the lower mantle, it is almost certainly accommodated primarily in minor hydrous phases, because the dominant lower mantle minerals (bridgmanite, ferropericlase, and calcium silicate perovskite) do not have the same capacity for water storage (Bolfan-Casanova et al. 2002, 2003; Panero et al. 2015). A plausible lower mantle host is the isostructural FeOOH-AlOOH-$MgSiO_4H_2$ system.

At moderate pressures (>6 GPa) goethite (α-FeOOH, space group $Pbnm$), a widespread iron oxy-hydroxide, transforms into ε-FeOOH, an orthorhombic (space group $P2_1nm$, $Z = 2$) phase composed of edge-sharing FeO_6 units that are close-packed along the c-axis, with hydrogen atoms occupying the channels between these close-packed octahedra (Bendeliani et al. 1972; Pernet et al. 1975; Bolotina et al. 2008) (Fig. 1a). At increased pressure, ε-FeOOH undergoes pressure-induced hydrogen-bond symmetrization resulting in a second-order phase transition (space group $Pnnm$, $Z = 2$) (Fig. 1c). However, the pressure at which this hydrogen bond symmetrization induced $P2_1nm \rightarrow Pnnm$ transition occurs remains contested (Gleason et al. 2013; Xu et al. 2013; Thompson et al. 2017; Ikeda et al. 2019). At the pressures of the Earth's lower mantle, ε-FeOOH forms a solid solution with δ-AlOOH and phase H ($MgSiH_2O_4$), creating a viable hydrogen reservoir with P-T stability extending from lower mantle conditions to those of the core-mantle boundary (Sano et al. 2008; Nishi et al. 2015; Xu et al. 2019).

Hydrogen bond symmetrization is the process by which the hydrogen in an asymmetrical O–H···O bonding unit becomes centered with respect to the two O atoms with increased pressure, as the longer hydrogen bridge bond (H···O) compresses more rapidly than the shorter but stiffer hydroxyl bond (O–H) (Holzapfel 1972).

* E-mail: ecthomps@sewanee.edu. ORCID 0000-0002-5944-5595
† Special collection papers can be found online at http://www.minsocam.org/MSA/AmMin/special-collections.html.

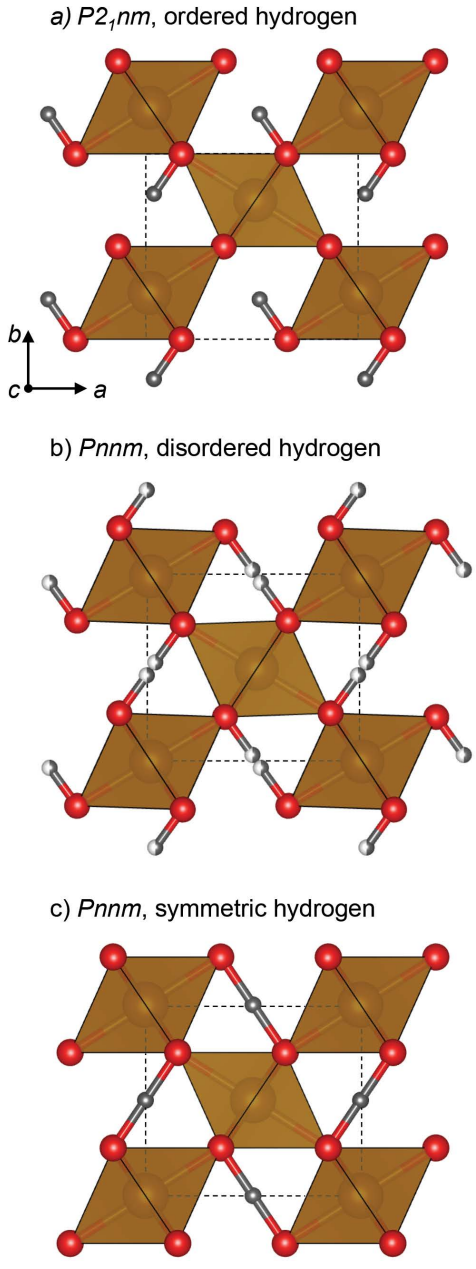

Figure 1. Low and moderate pressure structures of ε-FeOOH including the (**a**) $P2_1nm$ structure with ordered hydrogen occupation and asymmetric hydrogen bonds, (**b**) *Pnnm* structure with disordered hydrogen (hydrogen positions are 50% occupied), and (**c**) *Pnnm* structure with symmetric hydrogen bonds. Dashed lines indicate unit cells, oxygen atoms are red spheres, hydrogen atoms are gray spheres, and FeO_6 units are tan polyhedra, which are stacked in edge-sharing chains parallel to the *c*-axis. Image generated in VESTA (Momma and Izumi 2008).

Once the hydrogen bond is "symmetrized," the two donor-acceptor distances are equivalent, and this shift in charge balance can lead to additional subtle structural changes (Fig. 1c). In ε-FeOOH and other isostructural MOOH phases, the MO_6 octahedra shift from a slightly offset position to one centered along the twofold axis, leading to the increase in symmetry from $P2_1nm$ to *Pnnm* (e.g., Sano-Furukawa et al. 2009, 2012). Alternatively, proton disorder in which both hydrogen and iron atoms are disordered over symmetric positions on the twofold axis may also produce MOOH with *Pnnm* symmetry (Bolotina et al. 2008) with the resulting diffraction patterns nearly indistinguishable from symmetrized H-bond structures (e.g., Fujihara et al. 2002) (Fig. 1b). Importantly, a recent neutron diffraction study by Sano-Furukawa et al. (2018), found that in δ-AlOOH, which is isostructural to ε-FeOOH, proton disordering is a precursor to hydrogen bond symmetrization. Accurately determining the pressure at which hydrogen bond symmetrization occurs is important because the phenomenon is linked to changes in compressibility (Vanpeteghem et al. 2003; Tsuchiya et al. 2005; Hushur et al. 2011) and because isotopic effects may influence H/D fractionation in the deep Earth (e.g., Sano-Furukawa et al. 2009).

In addition to the previously described $P2_1nm \rightarrow Pnnm$ transition, ε-FeOOH reportedly undergoes a high-spin to low-spin transition, determined on the basis of X-ray diffraction (XRD) and X-ray emission spectroscopy (XES) experiments (Gleason et al. 2013). The XES results from Gleason et al. (2013) are indicative of a high-spin to low-spin transition initiated at ~40 GPa and completed at ~60 GPa. However, that study did not use a pressure-transmitting medium, which introduced significant deviatoric stress into the sample, inhibiting the detection of a sharp transition. A contemporary study by Xu et al. (2013), which used a pressure-transmitting medium, pinpointed this electronic transition more closely to ~45 GPa using a combination of Mössbauer spectroscopy, single-crystal diffraction, and resistivity measurements. In both studies, the authors propose causality between the hydrogen bond symmetrization and spin transition in ε-FeOOH, although Gleason et al. (2013) report that hydrogen bond symmetrization induces the spin transition, whereas Xu et al. (2013) conclude the spin transition induces hydrogen-bond symmetrization. However, both studies agree that a large (~11%) volume collapse occurs coincident with the high-spin to low-spin transition, attributable to an isostructural phase transition. Significant volume reductions have been previously reported due to high-spin to low-spin transitions without invoking hydrogen-bond symmetrization, although a volume reduction of ~11% is higher than the volume reductions reported for either ferropericlase [(Mg,Fe)O] (1–3%) or ferromagnesite [$(Mg,Fe)CO_3$] (6–10%) (Lin et al. 2013), possibly due to the larger relative volume occupied by iron atoms in FeOOH compared to these phases.

In this study, we present experimental evidence of two distinct transitions in ε-FeOOH in the explored pressure range (0–70 GPa): a low-pressure (~18 GPa) second-order transition connected to hydrogen bond symmetrization and an independent first-order transition at ~45 GPa. Additionally, we report evidence of a rapid reduction in the bandgap of ε-FeOOH at pressures consistent with the previously reported spin transition.

Methods

Synthesis of ε-FeOOH for this study was performed by Akio Suzuki and is described in Suzuki (2010). The high pressures necessary for this study were achieved by compressing ε-FeOOH samples using symmetric-type diamond-anvil cells (DACs) with 250 μm culet type II diamond anvils. Seventy-micrometer diameter sample chambers were laser ablated into stainless steel or rhenium gaskets pre-indented to 22 or 28 GPa, respectively. Powdered ε-FeOOH, kept in a desiccator

prior to loading, was pressed into platelets 3–5 μm thick and ~30 μm in diameter. Platelets of ε-FeOOH were loaded into the sample chamber, utilizing gas-loaded Ne or ~10 μm thick platelets of KBr as a pressure medium to reduce pressure gradients within the sample. Neon was loaded as a pressurized gas at the Advanced Photon Source using the COMPRES/GSECARS gas loading system (Rivers et al. 2008) and acted as a secondary pressure standard (Fei et al. 2007), with reported uncertainties based on the standard error of the (111), (200), and (220) *d*-spacings. Pressures were independently determined via the in situ monitoring of the R_1 luminescence line (Dewaele et al. 2008) of 2–3 ruby grains placed in the sample chamber, with errors reflecting the larger of either the standard deviation or 3%.

Room-temperature X-ray diffraction experiments were performed at beamline 13-ID-D (GSECARS) at the Advanced Photon Source, Argonne National Laboratory. A monochromatic (λ = 0.3344) incident X-ray beam was used, measuring 3 μm by 4 μm at full-width at half maximum of the focused spot. Sample-to-detector distances and tilt were calibrated using 1-bar diffraction of LaB_6. Diffraction patterns were integrated to produce 2θ plots using DIOPTAS (Prescher and Prakapenka 2015), positions of individual diffraction peaks were determined using PeakFit (Systat Software), and lattice parameters were calculated from the fitted *d*-spacings using the author's own Mathematica script. Individual peaks were fit to single Gaussian curves, and unresolved overlapping peaks were not used in the calculation of lattice parameters. All samples prepared for X-ray diffraction experiments were loaded using Ne as a pressure medium.

Fourier transform infrared (FTIR) spectra in this study were collected using both synchrotron and globar sources. Synchrotron experiments were performed at the 1.4.3 beamline of the Advanced Light Source at Berkeley Laboratory using a Nicolet 760 FTIR spectrometer with a custom microscope and HgCdTe detectors. Offline experiments were performed at Brookhaven National Laboratory using a Bruker Vertex 80v spectrometer and Hyperion 2000 microscope with an MCT detector. All FTIR spectra presented here reflect a spectral resolution of 4 cm^{-1}, measured wavelength ranges of 500 to 8000 cm^{-1}, and were recorded as 1024 or 512 scans. PeakFit was used for background subtraction and to obtain precise absorption peak positions using a least-squares refinement, and interference fringes in absorbance spectra were reduced mathematically in DatLab. Samples prepared for FTIR experiments used either Ne or KBr as pressure medium, and the three samples that went to the highest pressures used KBr.

Optical absorption measurements were collected at the University of Chicago. Spectra were recorded from 420 to 980 nm using a 0.3 m focal length Princeton Instruments SP-2300i spectrograph. Transmitted light (I), generated with a tungsten filament bulb, was measured through the pressure medium (KBr) only, while incident light (I_0) was collected through the sample and pressure medium. Background measurements were collected both with the light source off and with the light source on but measured at the gasket, which is opaque, with comparable results. Interference fringes in the absorbance spectra were removed mathematically in DatLab. To account for variation in sample thickness (h), reported absorption values [$\alpha = h^{-1}\ln(I_0/I)$] have been scaled such that I_0/I is equal for all samples at 10 GPa. Samples prepared for optical absorption measurements used KBr as pressure medium.

Results and Discussion

X-ray diffraction

High-pressure, room-temperature X-ray diffraction (XRD) measurements were used to re-evaluate the phase diagram of FeOOH up to 75 GPa, as the existing literature exhibits a paucity of volume-pressure (*V*-*P*) data in the mid-pressure range (20–50 GPa) (Gleason et al. 2008, 2013; Suzuki 2010, 2016; Ikeda et al. 2019). Additionally, using a gas-membrane diaphragm to remotely pressurize the DAC between diffraction measurements without manual action, data could be collected with greater pressure resolution than in previous studies. As X-ray diffraction inherently relies on electron density, the detection of hydrogen using powder XRD is virtually impossible. The $P2_1nm \rightarrow Pnnm$ transition is primarily defined by the pressure-induced symmetrization of the hydrogen bonds but associated with hydrogen bond disordering and symmetrization are subtle changes in the structure and strain accommodation, which enable the detection of these transitions indirectly (e.g., Sano-Furukawa et al. 2009, 2012; Kuribayashi et al. 2014).

In the lower pressure interval (0.5–43 GPa) the lattice parameters of ε-FeOOH were determined using at a minimum the (110), (101), (011), (020), (210), (211), (121), (220), (002), and (301) *hkl* peaks. The resulting unit-cell volumes and lattice parameters are plotted in Figures 2a and 2b and are reported in tabulated form in Supplemental[1] Table S1. The measured lattice parameters and unit-cell volumes of ε-FeOOH in this pressure interval are in excellent agreement with the results of Suzuki (2010, 2016) and Ikeda et al. (2019), albeit slightly lower than those reported by the Gleason et al. (2013). The diffraction data from Gleason et al. (2013) exhibit more scatter, likely due to the lack of pressure medium in that study, which likely contributed to the slight offset in measured *P*-*V* values.

Based on the Bragg peaks indexed in this study, the $P2_1nm$ and *Pnnm* structure cannot be distinguished from one another, as even at the lowest pressures of this study no peaks were observed that violated the additional systematic absences characteristic of the *Pnnm* symmetry ($h + l$ = odd for $h0l$, $k + l$ = odd for $0kl$). Additionally, based on the findings of Sano-Furukawa et al. (2009), who evaluated the $P2_1nm \rightarrow Pnnm$ transition in isostructural δ-AlOOH, the volume reduction associated with this second-order transition is likely unresolvable, rendering determinations of this phase boundary on this basis alone dubious. Thus, employing the approach of Sano-Furukawa et al. (2009, 2012), we evaluated the ratios of lattice parameters as a means of elucidating the subtle $P2_1nm \rightarrow Pnnm$ transition.

The evolution of the *a*/*b* and *b*/*c* lattice parameter ratios (Figs. 2c and 2d) reveal a change in the axial compression of ε-FeOOH with pressure, and the inflection points evident at 18 ± 1 GPa indicate a shift in the accommodation of strain in this system. Similar changes in axial compression have been used previously as an indicator of second-order phase changes in similar materials (e.g., Sano-Furukawa et al. 2009, 2012; Kuribayashi et al. 2014). On the basis of these lattice parameter ratios, we confirm that ε-FeOOH undergoes a second-order phase transition from the $P2_1nm$ to *Pnnm* structure at 18 ± 1 GPa, in good agreement with previous predictions based on density functional theory-based calculations (Thompson et al. 2017) and recent experiments (Ikeda et al. 2019). As any volume reduction across this presumed phase boundary is minimal (Fig. 2a), the *V*-*P* data from the entire pressure interval (0 to 45 GPa) was fit to a third-order Birch-Murnaghan equation of state (EoS) (Birch 1978):

$$P(V,T) = 3K_0 f_E \left[\left(1 + 2f_E\right)^{\frac{5}{2}} \left(1 + \frac{3}{2}\left[K_0' - 4\right] f_E\right)\right]$$

which relates pressure (P), volume (V), ambient pressure bulk modulus (K_0), and its pressure derivative (K_0') in terms of finite Eulerian strain (f_E):

$$f_E = \frac{1}{2}\left[\left(\frac{V_0}{V}\right)^{\frac{2}{3}} - 1\right]$$

which is a measure of the volume compression of a solid relative to its initial volume (V_0). Residuals from this fit are shown in Supplemental[1] Figure S1.

To obtain EoS parameters with the most comprehensive data set available, the *V*-*P* data from this study and Suzuki (2010, 2016) were combined, and the resultant equation of state pa-

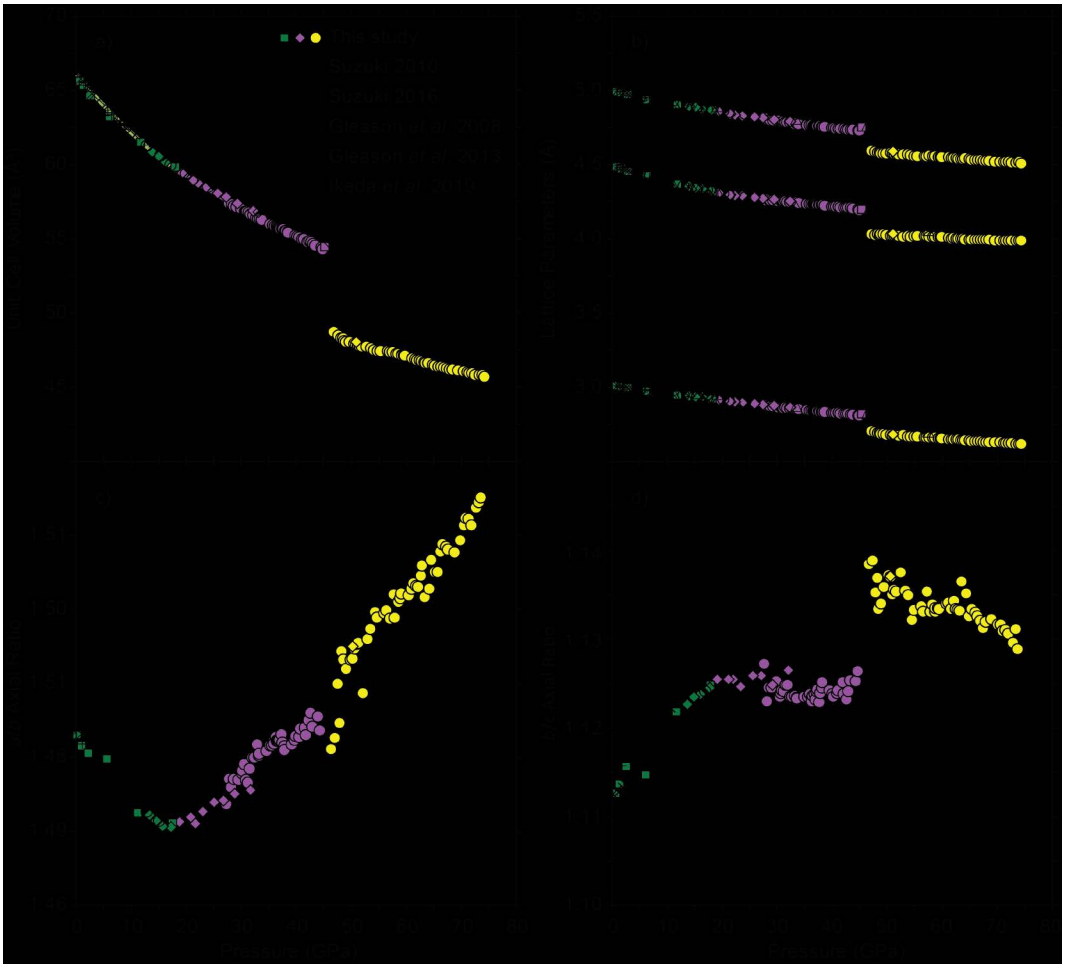

Figure 2. (**a**) Unit-cell volume, (**b**) lattice parameters, (**c**) *a*/*b*, and (**d**) *b*/*c* lattice parameter ratios of FeOOH as a function of pressure, including this study (solid symbols), Suzuki (2010) (black crosses), Suzuki (2016) (black X's), Gleason et al. (2008) (open diamonds), Gleason et al. (2013) (open triangles), and Ikeda et al. (2019) (open circles). Different solid symbols (circles, diamonds, squares) are used to show replicate samples in this study. Green, purple, and yellow symbols indicate that Braggs peaks have been indexed to the $P2_1nm$ (green), high-spin *Pnnm* (purple), and low-spin *Pnnm* (yellow) structures. Light green and light purple lines in **a** represent the equations of state using the parameters from lines 3 and 4 of Table 1, respectively. Error bars reflect uncertainties in the lattice parameters from this study, and when not visible reflect that errors are smaller than the symbols.

rameters are presented alongside parameters fit to the data from only this study. In addition to fitting *V*-*P* data from the entire 0–45 GPa pressure range, we also report EoS parameters derived from fitting the *V*-*P* data of the $P2_1nm$ and *Pnnm* structures separately. The resultant EoS parameters, as well as previously published results, are reported in Table 1. We find that EoS parameters derived from fitting the combined data set across the entire pressure range (0–45 GPa) are in reasonable agreement with those reported by Gleason et al. (2008) and Suzuki (2010, 2016). However, fitting *V*-*P* data for the $P2_1nm$ and *Pnnm* structures independently (using a fixed K_0' value of 4 because fewer fitted parameters are justified over the limited pressure ranges), reveals that the P*nnm* structure has a bulk modulus ~20% higher than that of the $P2_1nm$ ε-FeOOH, in good agreement with the ~19% predicted from DFT calculations (Thompson et al. 2017). These findings are also in good agreement with a prior study by Xu et al. (2013) that identified a reduction in the compressibility of FeOOH at ~16 GPa but did not connect this change in material properties to the onset of pressure-induced hydrogen-bond symmetrization or proton disordering. Similar increases in bulk modulus have been reported for other hydrous phases due to the onset of pressure-induced hydrogen-bond symmetrization or proton disordering (Vanpeteghem et al. 2003; Tsuchiya et al. 2005; Hushur et al. 2011).

Additionally, XRD data from this study revealed a second, independent structural transition in ε-FeOOH at ~45 GPa. The transition occurs over a small (<3 GPa) pressure interval and is evident in the appearance of multiple new Braggs peaks and a simultaneous reduction in the intensity, and eventual disappearance, of the Braggs peaks of the high-spin *Pnnm* structure (Fig. 3). This high-pressure (>45 GPa) structure of FeOOH is stable at ambient temperatures and pressures exceeding 70 GPa. While an earlier study identified a potential unit-cell volume reduction in this pressure range (Gleason et al. 2013), the

Table 1. Birch-Murnaghan equation of state (EoS) parameters of ε-FeOOH, including ambient-pressure unit volume (V_0), bulk modulus (K_0), and the pressure derivative of the bulk modulus (K_0') as well as the pressure range of the included room-temperature XRD data and the number of *V-P* data points included in each EoS fitting

	P (GPa)	No. data points	V_0 (Å^3)	K_0 (GPa)	K_0'
This study	0 to 45	59	65.87(3)	152(4)	4.9(2)
This study	0 to 45	59	65.57(6)	170(1)	4 (fixed)
This study, Suzuki (2010, 2016)	0 to 45	80	66.15(5)	141(3)	5.4(2)
This study, Suzuki (2010, 2016)	0 to 45	80	65.88(4)	163(1)	4 (fixed)
This study, Suzuki (2010, 2016) (*P*2$_1$*nm*)	0 to 16	29	66.14(4)	146(2)	4 (fixed)
This study (*Pnnm*)	18 to 45	50	65.3(1)	176(3)	4 (fixed)
Gleason et al. (2008)	8 to 17	9	66.3(5)	158(5)	4 (fixed)
Suzuki (2010)	0 to 9	8	66.20(3)	126(3)	10(1)
Suzuki (2016)	0 to 11	13	66.278(6)	135(3)	6.1(9)

Notes: The first and second lines are parameters obtained from fitting the same data to second- and third-order BM EOSs, respectively. Values in parentheses are uncertainties on the last digit. Residuals from the fit to a third-order Birch-Murnaghan equation of state are shown in Supplemental[1] Figure S1.

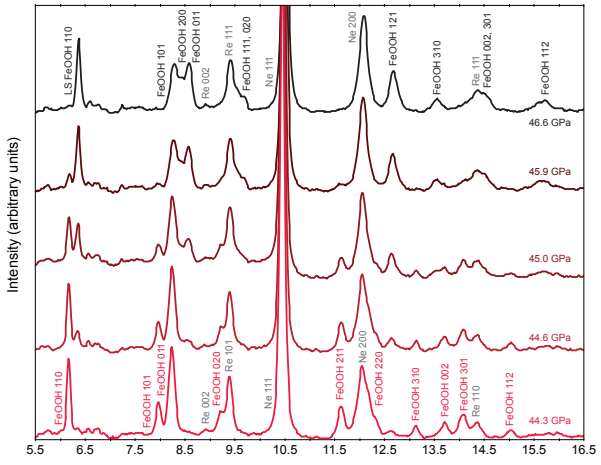

Figure 3. Integrated X-ray diffraction patterns of FeOOH at five increasing pressure steps from bottom to top: 44.3 GPa (red), 44.6, 45.0, 45.9, and 46.6 GPa (black), illustrating the structural transition in this pressure interval. Miller indices of ε-FeOOH are shown in red for the lower-pressure *Pnnm* structure, and in black for the higher-pressure, presumably low-spin, structure that is ~10% smaller. The Miller indices for the pressure medium (Ne) and gasket material (Re) are shown in gray.

improved pressure resolution of the current study clarifies the pressure at which this transition occurs. The sharpness of this phase boundary and the significant volume reduction contrast with the gradual, displacive second-order transition produced by the gradual change in charge density due to hydrogen bond symmetrization. Conversely, the structural transition observed at ~45 GPa is within the pressure range in which the high-spin to low-spin transition has been observed (Gleason et al. 2013), and the contraction of the Fe^{3+} ionic radius across the high-spin to low-spin transition has been reported to produce significant volume reductions in other iron-bearing minerals (e.g., Lin et al. 2013). Although the <3 GPa interval in which the first-order transition is observed in this study is significantly narrower than the 20 GPa pressure interval across which the high-spin to low-spin transition was reported (Gleason et al. 2013), this discrepancy may be due to the lack of a pressure medium in the earlier study, an omission that can produce pressure gradients that can lead to significantly broader spin transitions.

High-pressure (>45 GPa) X-ray diffraction data from this study were indexed to a *Pnnm* (Z = 2) unit cell, using at a minimum the (110), (200), (011), (121), (310), (301), and (112) *d*-spacings. The resultant lattice parameters and unit-cell volumes are consistent with a volume reduction of 10% without a loss of symmetry, in reasonable agreement with the isostructural, 11% volume collapse proposed by Gleason et al. (2013) (Fig. 2a). However, a recent ab initio study has predicted an intermediate *Pbca* (Z = 8) structure is stable between the *Pnnm* and the pyrite ($Pa\bar{3}$) phases of AlOOH (Verma et al. 2018). The high-pressure (>45 GPa) XRD data from this study was indexed to the proposed *Pbca* structure, but the reduction in volume across this potential *Pnnm* → *Pbca* transition appears implausibly large (26%) and resulted in a reduced quality of fit. An attempt was made to index the high-pressure Bragg peaks to the α-PbO_2 structure (*Pbcn*) adopted by $CaCl_2$-type (*Pnnm*) oxides at high pressures, but this failed to produce a reasonable fit to the data. Additionally, we can definitively state that this is not the appearance of the high-pressure pyrite structure of FeOOH, to which ε-FeOOH is expected to transition at comparable pressures and elevated temperatures (Nishi et al. 2017; Hu et al. 2016). Therefore, we interpret the first-order transition at 45 ± 2 GPa as an isostructural volume collapse (i.e., *Pnnm* → *Pnnm*), accompanied by an increase in the *a*/*b* ratio in the higher-pressure structure (Fig. 2d). The change in the *a*/*b* ratio may be due to a relaxation of the distortion of the FeO_6 units, in agreement with Xu et al. (2013) and linked to the previously reported high-spin to low-spin transition (Gleason et al. 2013; Xu et al. 2013). In the future, single-crystal X-ray diffraction structure refinements might help elucidate the nature of this structural transition (displacive vs. reconstructive) and refine the symmetry of the high pressure, low-spin structure.

Infrared and visible absorption spectroscopy

Room-temperature infrared absorption spectra of ε-FeOOH were collected at ambient pressure and at regularly increasing pressure intervals of ~2 GPa up to ~50 GPa. Qualitatively, the ambient pressure ε-FeOOH spectrum bears similarity to that of *P*2$_1$*nm* β-CrOOH, with which ε-FeOOH is isosymmetric (Jahn et al. 2012) (Fig. 4). At ambient pressure, the O–H stretching region presents as a broadband feature (2600–3100 cm^{-1}), consistent with previously reported spectra of the low-pressure polymorphs of FeOOH (e.g., Williams and Guenther 1996; Kagi et al. 2008), and with increased pressure, the broadband O–H stretching region further broadens and shifts to lower wavenumbers. Unfortunately, the increased breadth of the O–H stretching feature and its increased proximity to the diamond absorption region prevent tracking the pressure dependence of this feature above ~17 GPa. Although the O–H stretching band could only be monitored over a limited pressure range, its negative frequency shift pressure dependence was clearly observable at low pressures (Supplemental[1] Fig. S3). A linear fit of the pressure-frequency data of the O–H stretching band results in an approximate pressure dependence of –14 cm^{-1} GPa^{-1}, demonstrative of a softening behavior consistent with eventual

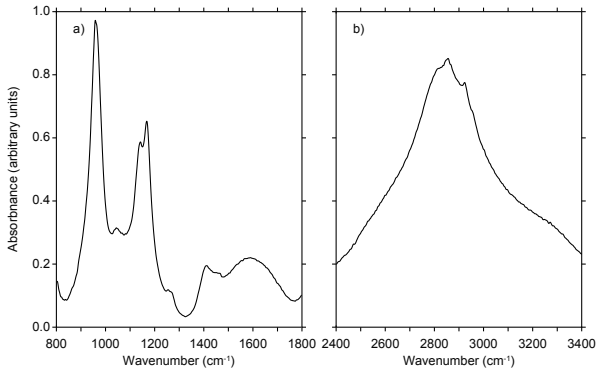

Figure 4. Ambient pressure infrared spectra of $P2_1nm$ ε-FeOOH in the (**a**) lattice and OH-bending vibrations region and (**b**) OH-stretching region.

hydrogen-bond symmetrization. However, it is not feasible to predict the pressure of eventual hydrogen-bond symmetrization, as the relationship between the 1-bar stretching frequency and O–H pressure dependence is poorly understood in ε-FeOOH and similarly structured phases, and the pressure range of available ε-FeOOH O–H stretching frequency data is limited.

The ambient-pressure infrared spectrum of ε-FeOOH also contains three distinct absorption bands at 965, 1145, and 1175 cm^{-1} that were identified as O–H bending vibrations based on comparison to similar structures (Williams and Guenther 1996; Mashino et al. 2016; Pinney and Morgan 2013). Spectra at successive pressure steps were evaluated to determine the frequency shifts in the O–H bending as a function of pressure (Fig. 5). As with the OH-stretching region, these features broaden with increased pressure, and the two higher-frequency bands become indistinguishable above 17.5 ± 1 GPa. The lowest-frequency bending band remains distinct to higher pressures, but the pressure dependence of this band changes dramatically above 17.5 ± 1 GPa. The sudden change in the pressure dependence of this band suggests a reorientation of the O–H bonds, suggestive of the onset of pressure-induced hydrogen-bond symmetrization or proton disordering. A similar shift in the pressure dependence of the OH-absorption bands in isostructural δ-AlOOH was observed by Kagi et al. (2010) at ~10 GPa, consistent with the onset of proton disordering in that phase (Sano-Furukawa et al. 2018).

During the course of these IR measurements, a reduction in the transmitted IR signal was observed in ε-FeOOH samples compressed above ~40 GPa (Supplemental[1] Fig. S4). In addition to the changes in IR transmission properties, changes in the optical properties of FeOOH were observed upon compression. The samples were translucent orange at ambient and low pressures, but reddened with increased pressure and became opaque to transmitted visible light at 45 GPa, slightly preceding the loss of IR transmission (Supplemental[1] Fig. S4). To quantify these observations, visible to near-infrared absorption measurements of ε-FeOOH were collected up to pressures exceeding 70 GPa, to track the pressure dependence of the absorption edge. Representative high-pressure optical absorption spectra of ε-FeOOH are shown in Figure 6a and indicate a systematic pressure-induced increase in absorption concordant with qualitative observations. Normalized data for five samples are plotted in Figure 6b, in which there are two key features. First, each sample underwent

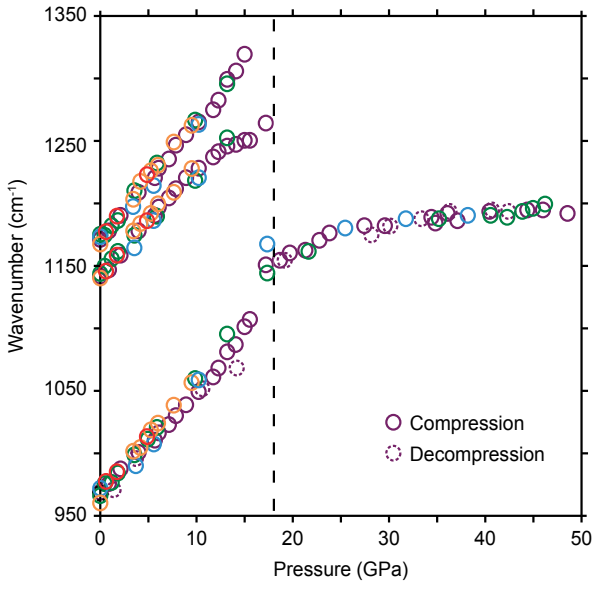

Figure 5. Evolution of the O–H bending frequencies of FeOOH as a function of pressure. The pressure of the $P2_1nm \rightarrow Pnnm$ transition is indicated by a black dashed line. Different colors are used to distinguish the five replicate samples from this study using either Ne as a pressure medium (red, orange) or KBr as a pressure medium (green, blue, purple).

a transient minimum in optical transmission between 15–20 GPa before gradually recovering to previous values over the subsequent ~5 GPa. Second, all five samples became opaque in the light range probed (1.45 to 2.05 eV) above 45.7 GPa (Fig. 6b), above which the ratio of transmitted light (I) to incident light (I_0) that can propagate through the sample decreases to zero. These vis/NIR absorption findings suggest a significant reduction in the bandgap in this pressure interval.

Implications

Close evaluation of the high-pressure behavior of ε-FeOOH at ambient temperature indicates two sequential, structural phase transitions in the 0–75 GPa pressure range. A second-order transition at 18 ± 1 GPa was determined on the basis of three observations: (1) a change in axial compressibility evident in the lattice parameter ratios measured using powder XRD; (2) a change in the OH-bending modes observed with FTIR spectroscopy; and (3) a transient decrease in optical absorption. In accordance with the previous work of Sano-Furukawa et al. (2009, 2012, 2018) that evaluated isostructural MOOH phases, this 18 ± 1 GPa transition is the $P2_1nm \rightarrow Pnnm$ transition produced by either pressure-induced hydrogen-bond symmetrization or proton disordering, with future neutron diffraction work needed to differentiate between these mechanisms. Furthermore, this transition is observed to lead to a ~20% increase in bulk modulus and could be linked to the increase in compressional velocity (V_P) reported by Ikeda et al. (2019).

At 45 ± 2 GPa, *Pnnm* ε-FeOOH undergoes a first-order structural phase transition, identifiable due to the appearance of new Bragg peaks coincident with the disappearance of the high-spin *Pnnm* peaks. This high-pressure structure of FeOOH

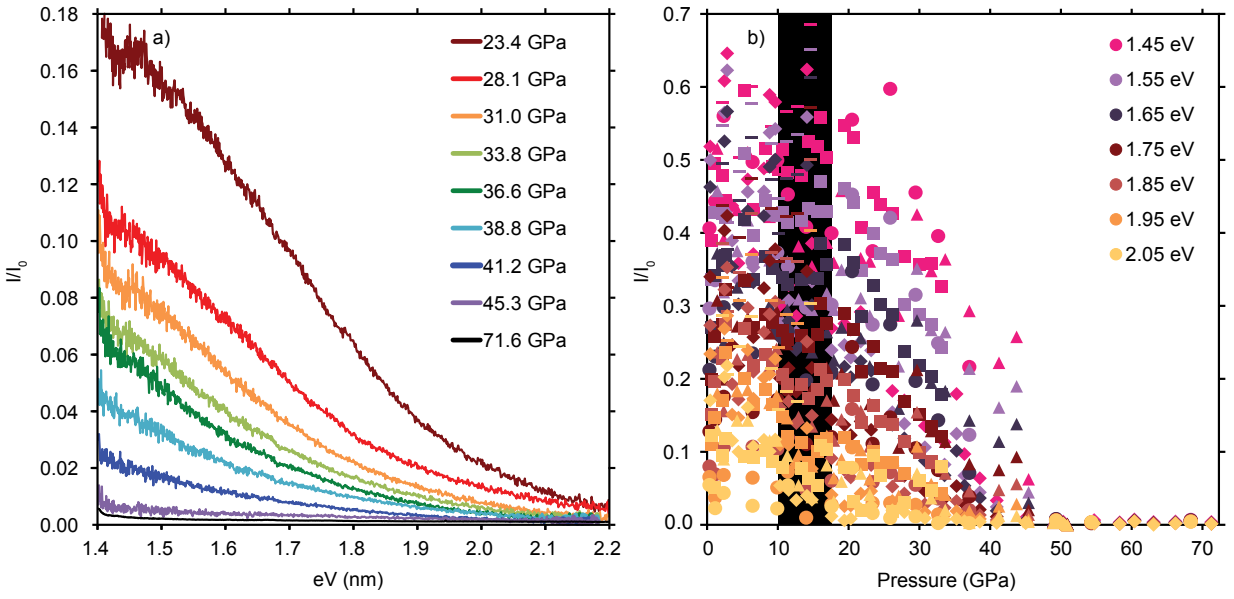

Figure 6. Optical absorption data, including (**a**) representative optical transmission spectra, indicating the pressure-dependent increase in the absorption of ε-FeOOH, and (**b**) data from five samples of ε-FeOOH, each indicated with a different symbol (diamonds, squares, circles, triangles, and horizontal dashes), showing the change in the ratio of transmitted light (I) to incident light (I_0) as a function of pressure (X-axis) and the wavelength of the incident light, which is indicated by color.

can also be indexed to *Pnnm* with a ~10% volume reduction, in good agreement with previous studies (Gleason et al. 2013; Xu et al. 2013). Therefore, we propose that the first-order transition at 45 ± 2 GPa is a nearly isostructural S volume collapse (i.e., *Pnnm* → *Pnnm*), accompanied by a small (~1%) increase in the *a*/*b* ratio in the higher-pressure structure (Fig. 2d). As such, low-spin *Pnnm* FeOOH is stable across a wide pressure range (more than 30 GPa). However, the phase diagram of FeOOH at high pressures and moderate temperatures should be assessed to determine the relevance of low-spin *Pnnm* FeOOH to the Earth's interior, as the formation of the pyrite ($Pa\bar{3}$) structure is reported at comparable pressures and high temperatures (Nishi et al. 2017; Hu et al. 2016). In the future, single-crystal X-ray diffraction structure refinements may be beneficial in verifying the symmetry of this higher pressure, low-spin structure.

In addition to the first-order structural transition identified in FeOOH at ~45 GPa, a color change (translucent orange to black) was observed at high pressure, and the optical opacity of *Pnnm* ε-FeOOH was quantified using visible/NIR transmission and infrared absorption. Visible to near-infrared absorption measurements of ε-FeOOH also identified a systematic pressure-induced increase in absorption consistent with band gap reduction in the high-spin *Pnnm* phase, although complete band gap collapse (i.e., metallization) of this phase cannot be established on the basis of these experiments alone. FeOOH becomes opaque in the 1.45–2.05 eV range and also in the mid-IR at ~45 GPa, indicating a change in optical properties along with the high-spin to low-spin transition in this material, as both phenomena are tied to changes in the d orbitals of the iron atoms. In fact, a similar increase in optical opacity has been previously linked to the high-spin to low-spin transition in siderite (Lobanov et al. 2015) and ferropericlase (Keppler et al. 2007). The apparent width of this transition, when compared to the sharpness of the structural transition observed using diffraction, may be attributable to the difference in the hydrostaticity of the pressure medium (KBr and Ne, respectively).

These results demonstrate that bandgap reduction, the previously observed high-spin to low-spin spin transition (Gleason et al. 2013; Xu et al. 2013), and the first-order phase transition in ε-FeOOH all occur at a pressure (45 ± 2 GPa) greatly exceeding the $P2_1nm$ → *Pnnm* symmetry transition associated with a change in hydrogen bonding (18 ± 1 GPa). Therefore, hydrogen-bond symmetrization is not the driver of spin transition in ε-FeOOH or vice versa. Rather, FeOOH undergoes a second-order $P2_1nm$ → *Pnnm* symmetry change caused by a shift in hydrogen bonding at 18 GPa, and a subsequent, unrelated first-order transition at 45 GPa that involves a significant volume change, spin transition, and optical opacity. Furthermore, although end-member ε-FeOOH is expected to transition to the pyrite ($Pa\bar{3}$) structure at the concurrent pressures and high temperatures of the Earth's mantle (Nishi et al. 2017; Hu et al. 2016), aluminum substitution is expected to increase the thermodynamic stability of (Fe,Al)OOH such that the low-spin *Pnnm* structure may be stable at the conditions of the deep Earth (e.g., Nishi et al. 2015; Xu et al. 2019). We anticipate that the high-spin to low-spin spin transition and associated volume collapse in intermediate compositions in the FeOOH-AlOOH-$MgSiH_2O_4$ system are likely to occur at lower pressures than in the Fe-end-member, as has been observed in ferropericlase (Fei et al. 2007). Additional experiments are needed to assess the influence of cation substitution on the phase boundaries of the FeOOH-AlOOH-$MgSiO_4H_2$ system, as this may play a pivotal role in the transport of water (OH^-) deep into the Earth's lower mantle (Ohira et al. 2014; Xu et al. 2019) and may contribute to geophysical heterogeneities observed in the deep Earth (Thompson et al. 2017; Ohira et al. 2019).

Acknowledgments and Funding

The authors declare no real or perceived financial conflicts of interest related to this work. Supporting information can be found in the Supplemental Materials[1]. The authors thank M.M. Reagan for providing sample material, which was originally synthesized by A. Suzuki. This work was supported by a National Science Foundation (NSF) EAR Postdoctoral Fellowship under grant EAR-1725673 for E.C.T. and NSF grant EAR-1651017 for A.J.C. The FTIR facilities at the National Synchrotron Light Source is supported by Consortium for Materials Properties Research in Earth Sciences (COMPRES) under NSF Cooperative Agreement EAR-1143050 and by the U.S. Department of Energy, Office of Science, Office of Basic Energy Sciences, under contract DE-AC02-98CH10886. Use of the COMPRES-GSECARS gas loading system was supported by COMPRES under NSF Cooperative Agreement EAR-1606856 and by GSECARS through NSF grant EAR-1634415 and DOE grant DE-FG02-94ER14466. This research used resources of the Advanced Photon Source, a U.S. Department of Energy (DOE) Office of Science User Facility operated for the DOE Office of Science by Argonne National Laboratory under contract DE-AC02-06CH11357. We also thank three anonymous reviewers whose comments helped improve this manuscript.

References cited

Bendeliani, N.A., Baneyeva, M.I., and Poryvkin, D.S. (1972) Synthesis of a new modification of FeO(OH) stable at high pressures. Geokhimiya, 7, 871–873. AN: 020182293.

Birch, F. (1978) Finite strain isotherm and velocities for single crystal and polycrystalline NaCl at high-pressures and 300 K. Journal of Geophysical Research, 83, 1257–1268. doi:10.1029/JB083iB03p01257.

Bolfan-Casanova, N., Mackwell, S.J., Keppler, H., McCammon, C.A., and Rubie, D.C. (2002) Pressure dependence of H solubility in magnesiowüstite up to 25 GPa: Implications for the storage of water in the Earth's lower mantle. Geophysical Research Letters, 29(10), 891–894. doi:10.1029/2001GL014457.

Bolfan-Casanova, N., Keppler, H., and Rubie, D.C. (2003) Water partitioning at 660 km depth and evidence for very low water solubility in magnesium silicate perovskite. Geophysical Research Letters, 30(17), 1905. doi:10.1029/2003GL017182.

Bolotina, N., Molchanov, V., Dyuzheva, T., Lityagina, L., and Bendeliani, N. (2008) Single-crystal structures of high-pressure phases FeOOH, FeOOD, and GaOOH. Chrystallography Reports, 53, 960. doi:10.1134/S1063774508060084.

Dewaele, A., Torrent, M., Loubeyre, P., and Mezouar M. (2008) Compression curves of transition metals in the Mbar range: Experiments and projector augmented-wave calculations. Physical Review B, 78, 104102. doi:10.1103/PhysRevB.78.104102.

Dixon, J.E., Dixon, T.H., Bell, D.R., and Malservisi, R. (2004) Lateral variation in upper mantle viscosity: Role of water. Earth and Planetary Science Letters, 222, 451–467. doi:10.1016/j.epsl.2004.03.022.

Fei, Y., Ricolleau, A., Frank, M., Mibe, K., Shen, G., and Prakapenka, V. (2007) Toward an internally consistent pressure scale. Proceedings of the National Academy of Sciences, 104(22), 9182–9186. doi:10.1073/pnas.0609013104.

Fujihara, T., Ichikawa, M., Gustafsson, T., Olovsson, I., and Tsuchida, T. (2002) Powder-neutron diffraction studies of geometric isotope and hydrogen-bonding effects in β-CrOOH. Journal of Physics and Chemistry of Solids, 63, 309–315. doi:10.1016/S0022-3697(01)00147-0.

Gleason, A., Jeanloz, R., and Kunz, M. (2008) Pressure-temperature stability studies of FeOOH using X-ray diffraction. American Mineralogist, 93, 1882–1885. doi:10.2138/am.2008.2942.

Gleason, A., Quiroga, C., Suzuki, A., Pentcheva, R., and Mao, W. (2013) Symmetrization driven spin transition in ε-FeOOH at high pressure. Earth and Planetary Science Letters, 379, 49–55. doi:10.1016/j.epsl.2013.08.012.

Hirschmann, M. (2006) Water, melting, and the deep Earth H_2O cycle. Annual Review of Earth and Planetary Sciences, 34, 629–653. doi:10.1146/annurev.earth.34.031405.125211.

Holzapfel, W.B. (1972) On the symmetry of the hydrogen bonds in ice VII. The Journal of Chemical Physics, 56, 712. doi:10.1063/1.1677221.

Hu, Q., Kim, D., Liu, J., Meng, Y., and Mao, H.-K. (2016) FeO_2 and FeOOH under deep lower-mantle conditions and Earth's oxygen-hydrogen cycles. Nature, 534, 241–245. doi:10.1038/nature18018.

Hushur, A., Manghnani, M.H., Smyth, J.R., Williams, Q., Hellebrand, E., Lonappan, D., Ye, Y., Dera, P., and Frost, D.J. (2011) Hydrogen bond symmetrization and equation of state of phase D. Journal of Geophysical Research, 116, B06203. doi:10.1029/2010JB008087.

Ikeda, O., Sakamaki, T., Ohashi, T., Goto, M., Higo, Y., and Suzuki, A. (2019) Sound velocity measurements of ε-FeOOH up to 24 GPa. Journal of Mineralogical and Petrological Sciences. doi:10.2465/jmps.181115b.

Jahn, S., Wunder, B., Kock-Müller, M., Tarrieu, L., Pöhle, M., Watenphul, A., and Taran, M. (2012) Pressure-induced hydrogen bond symmetrization in guyanaite, β-CrOOH: Evidence from spectroscopy and *ab initio* simulations. European Journal of Mineralogy, 24, 839–850. doi:10.1127/0935-1221/2012/0024-2228.

Kagi, H., Ushijima, D., Iizuka, R., Nakano, S., and Nagai, T. (2008) Micro-pellet method for infrared absorption spectroscopy using a diamond anvil cell under a quasi-hydrostatic condition. High Pressure Research, 28(3), 299–306. doi:10.1080/08957950802346868.

Kagi, H., Ushijima, D., Sano-Furukawa, A., Komatsu, K., Iizukam R., Nagai, T., and Nakano, S. (2010) Infrared absorption spectra of δ-AlOOH and its deuteride at high pressure and implication to pressure response of the hydrogen bonds. Journal of Physics: Conference Series, 215, 012052. doi:10.1088/1742-6596/215/1/012052.

Karato, S. (2010) Rheology of the deep upper mantle and its implications for the preservation of the continental roots: A review. Tectonophysics, 481, 82–98. doi:10.1016/j.tecto.2009.04.011.

Keppler, H., Kantor, I., and Dubrovisnky, L. (2007) Optical absorption spectra of ferropericlase to 84 GPa. American Mineralogist, 92, 433–436. doi:10.2138/am.2007.2454.

Kuribayashi, T., Sano-Furukawa, A., and Nagase, T. (2014) Observation of pressure-induced phase transition of δ-AlOOH by using single crystal synchrotron X-ray diffraction method. Physics and Chemistry of Minerals, 41, 303–312. doi:10.1007/s00269-013-0649-6.

Lin, J.-F., Speaziale, S., Mao, Z., and Marquardt, R. (2013) Effects of the electronic spin transitions of iron in lower mantle minerals: Implications for deep mantle geophysics and geochemistry. Reviews of Geophysics, 51(2), 244–275. doi:10.1002/rog.20010.

Liu, J., Hu, Q., Kim, D.Y., Wu, Z., Wang, W., Xiao, Y., Chow, P., Meng, Y., Prakapenka, V.B., Mao, H.-K., and Mao, W.L. (2017) Hydrogen-bearing iron peroxide and the origin of ultralow-velocity zones. Nature, 551, 494–497. doi:10.1038/nature24461

Lobanov, S.S., Goncharov, A.F., and Litasov, K.D. (2015) Optical properties of siderite ($FeCO_3$) across the spin transition: Crossover to iron-rich carbonates in the lower mantle. American Mineralogist, 100(5-6), 1059–1064.

Mashino, I., Murakami, M., and Ohtani, E. (2016) Sound velocities of δ-AlOOH up to core-mantle boundary pressures with implications for the seismic anomalies in the deep mantle. Journal of Geophysical Research: Solid Earth, 121, 595–609. doi:10.1002/2015JB012477.

Momma, K., and Izumi, F. (2008) VESTA: A three-dimensional visualization system for electronic and structural analysis. Journal of Applied Crystallography, 41, 653–658. doi:10.1107/S0021889808012016.

Nishi, M., Irifune, T., Greaux, S., Tange, Y., and Higo, Y. (2015) Phase transitions of serpentine in the lower mantle. Physics of the Earth and Planetary Interiors, 245, 52–58. doi:10.1016/j.pepi.2015.05.007.

Nishi, M., Kuwayama, Y., Tsuchiya, J., and Tsuchiya, T. (2017) The pyrite-type high-pressure form of FeOOH. Nature, 547, 205–208. doi:10.1038/nature22823.

Ohira, I., Ohtani, E., Sakai, T., Miyahara, M., Hirao, N., Ohishi, Y., and Nishijima, M. (2014) Stability of a hydrous δ-AlOOH-$MgSiO_2(OH)_2$, and a mechanism for water transport into the base of lower mantle. Earth and Planetary Science Letters, 401, 12–17. doi:10.1016/j.epsl.2014.05.059.

Ohira, I., Jackson, J.M., Solomatova, N.V., Sturhahn, W., Finkelsteinm G.J., Kamada, S., Kawazoe, T., Maeda, F., Hirao, N., Nakano, S., Toellner, T.S., Suzuki, A., and Ohtani, E. (2019) Compressional behavior and spin state of δ-(Al,Fe)OOH at high pressure. American Mineralogist, 104(9), 1273–1284. doi:10.2138/am-2019-6913.

Palot, M., Jacobsen, S.D., Townsend, J.P., Nestola, F., Marquardt, K., Miyajim, N., Harris, J.W., Stachel, T., McCammon, C.A., and Pearson, D.G. (2016) Evidence for H_2O-bearing fluids in the lower mantle from diamond inclusion. Lithos, 265, 237–243. doi:10.1016/j.lithos.2016.06.023.

Panero, W.R., Pigott, J.S., Reaman, D.M., Kabbes, J.E., and Liu, Z. (2015) Dry (Mg,Fe)SiO_3 perovskite in the Earth's lower mantle. Journal of Geophysical Research: Solid Earth, 100(2), 894–908. doi:https://doi.org/10.1002/2014JB011397.

Pearson, D.G., Brenker, F.E., Nestola, F., McNeill, J., Nasdala, L., Hutchison, M.T., Matveev, S., Mather, K., Silversmit, G., Schmitz, S., Vekemans, B. and Vincze, L. (2014) Hydrous mantle transition zone indicated by ringwoodite included within diamond. Nature, 507, 221–224. doi:10.1038/nature13080

Pernet, M., Joubert, J., and Berthet-Colominas, C. (1975) Etude par diffraction neutronique de la forme haute pression de FeOOH. Solid State Communications, 17, 1505–1510. doi:0.1016/0038-1098(75)90983-7.

Pinney, N., and Morgan, D. (2013) Ab initio study of structurally bound water at cation vacancy sites in Fe- and Al-oxyhydroxide materials. Geochimica et Cosmochimica Acta, 114, 94–111. doi:10.1016/j.gca.2013.03.032.

Prescher, C., and Prakapenka, V. (2015) DIOPTAS: A program for reduction of two-dimensional X-ray diffraction data and data exploration. High Pressure Research, 35(3), 223–230. doi:10.1080/08957959.2015.1059835.

Rivers, M., Prakapenka, V., Kubo, A., Pullins, C., Holl, C., and Jacobsen, S. (2008) The COMPRES/GSECARS gas-loading system for diamond anvil cells at the Advanced Photon Source. High Pressure Research, 28, 273–292. doi:10.1080/08957950802333593.

Sano, A., Ohtani, E., Kondo, T., Hirao, N., Sakai, T., Sata, N., Ohishi, Y., and Kikegawa, T. (2008) Aluminous hydrous mineral δ-AlOOH as a carrier of

hydrogen into the core-mantle boundary. Geophysical Research Letters, 35, L03303. doi:10.1029/2007GL031718.
Sano-Furukawa, A., Kagi, H., Nagai, T., Nakano, S., Fukura, S., Ushijim, D., Iizuka, E., and Yagi, T. (2009) Change in compressibility of δ-AlOOD and δ-AlOOH at high pressure: A study of isotope effect and hydrogen-bond symmetrization. American Mineralogist, 94, 1255–1261. doi:10.2138/am.2009.3109.
Sano-Furukawa, A., Yagi, T., Okada, T., Gotou, H., and Kikegawa, T. (2012) Compression behaviors of distorted rutile-type hydrous phases, MOOH (M = Ga, In, Cr) and CrOOD. Physics and Chemistry of Minerals, 39, 375–383. doi:10.1007/s00269-012-0487-y.
Sano-Furukawa, A., Hattori, T., Komatsu, K., Kagi, H., Nagai, T., Molaison, J.J., dos Santos, A.M., and Tulk, C.A. (2018) Direct observation of symmetrization of hydrogen bond in δ-AlOOH under mantle conditions using neutron diffraction. Scientific Reports, 8, 15520. doi:10.1038/s41598-018-33598-2.
Sarafian, E., Gaetani, G.A., Hauri, E.H., and Sarafian, A.R. (2017) Experimental constraints on the damp peridotite solidus and oceanic mantle potential temperature. Science, 355(6328), 942–945. doi:10.1126/science.aaj2165.
Syassen, K. (2012) Computer Code DATLAB, Max Planck Institute, Stuttgart, Germany.
Suzuki, A. (2010) High-pressure X-ray diffraction study of ε-FeOOH. Physics and Chemistry of Minerals, 37, 153–157. doi:10.1007/s00269-009-0319-x
——— (2016) Pressure-volume-temperature equation of state of ε-FeOOH to 11 GPa and 700 K. Journal of Mineralogical and Petrological Sciences, 111, 420–424. doi:10.2465/jmps.160719c.
Thompson, E., Campbell, A., and Tsuchiya, J. (2017) Elasticity of ε-FeOOH: Seismic implications for Earth's lower mantle. Journal of Geophysical Research: Solid Earth, 122(7), 5038–5047. doi:10.2138/am-2016-5465.
Tschauner, O., Haung, S., Greenberg, E., Prakapenka, V.B., Ma, C., Rossman, G.R., Shen, A.H., Zhang, D., Newville, M., Lanzirotti, A., and Tait, K. (2018) Ice-VII inclusions in diamonds: Evidence for aqueous fluid in Earth's deep mantle. Science, 359, 1136–1139. doi:10.1126/science.aao3030.
Tsuchiya, J., Tsuchiya, T., and Tsuneyuki, S. (2005) First-principles study of hydrogen bond symmetrization of phase D under high pressure. American Mineralogist, 90, 44–49. doi:10.2138/am.2005.1628.
van der Hilst, R.D., Widiyantoro, S., and Engdahl, E.R. (1997) Evidence for deep mantle circulation from global tomography. Nature, 386, 578–584. doi:10.1038/386578a0.
van der Meijde, M., Marone, F., Giardini, D., and van der Lee, S. (2003) Seismic evidence for water deep in the Earth's upper mantle. Science, 300, 1556–1558. doi:10.1126/science.1083636.
Vanpeteghem, C.B., Ohtani, E., Kondo, T., Takemura, K., and Kikegawa, T. (2003) Compressibility of phase Egg $AlSiO_3OH$: Equation of state and role of water at high pressure. American Mineralogist, 88, 1408–1411. doi:10.2138/am-2003–1002.
Verma, A.K., Modak, P., and Stixrude, L. (2018) New high pressure phases in MOOH (M = Al, Ga, In). American Mineralogist, 103, 1906–1917. doi:10.2138/am-2018-6634.
Williams, Q., and Guenther, L. (1996) Pressure-induced changes in the bonding and orientation of hydrogen in FeOOH-goethite. Solid State Communications, 100:2, 105–109. doi:10.1016/0038-1098(96)00374-2
Xu, C., Nishi, M., and Inoue, T. (2019) Solubility behavior of δ-AlOOH and ε-FeOOH at high pressures. American Mineralogist, 104, 1416–1420. doi:10.2138/am-2019-7064.
Xu, W., Greenberg, E., Rozenberg, G., Pasternak, M., Bykova, E., Boffa Ballaran, T., Dubrovinsky, L., Prakapenka, V., Hanfland, M., Vekilova, O., Simak, S., and Abrikosov, I. (2013) Pressure-induced hydrogen bond symmetrization in iron oxyhydroxide. Physical Review Letters, 111(17), 175501. doi:10.1103/PhysRevLett.111.175501.

Manuscript received February 9, 2020
Manuscript accepted June 10, 2020
Manuscript handled by Anne Peslier

Endnote:

[1]Deposit item AM-20-127468, Supplemental Figures and Tables. Deposit items are free to all readers and found on the MSA website, via the specific issue's Table of Contents (go to http://www.minsocam.org/MSA/AmMin/TOC/2020/Dec2020_data/Dec2020_data.html).